A Signal Processing Model for Laser Print Engines

Richard B. Wells, *Senior Member, IEEE,* Akaraphunt Vongkunghae, and Jang Yi, *Student Member, IEEE*

***Abstract*-- An accurate printer model that is efficient enough to be used by halftoning algorithms is proposed. The signal processing model (SPM) proposed in this paper utilizes a physical model to train Adaptive Linear Combiners (ALCs), after which the average exposure of each subpixel for any input pattern can be calculated using the optimized weight vector. The SPM can be used to model multi-level halftoning and resolution enhancement, as well as traditional halftoning . The SPM is comprised of a single layer of ALC's and is adapted using the LMS algorithm. A relatively small number of training patterns suffices to obtain adequate model accuracy.**

Index Terms—Adaptive linear combiner, electrophotography, LMS algorithm, printer model, signal processing model.

I. INTRODUCTION

The purpose of a printer model is to accurately predict the gray level of a binary image produced by a printer. Printer models are widely used in various digital halftoning algorithms, in which a continuous-tone image is transformed into a binary image. Halftoning is a necessary process for printing gray-scale images on paper since the direct rendition of gray tones on paper is otherwise impossible in electrophotography. In this paper, we introduce an approach to printer modeling based upon signal processing techniques.

In recent years, there has been increasing interest in digital halftoning to efficiently improve the print quality of laser printers using printer models. Pappas and Neuhoff proposed a circular dot-overlap printer model [1]. It accounts for dot-overlap distortions by assigning a constant gray-scale value for a pixel within the pixel boundary based on the pixel's on/off status and the interaction of its eight neighboring pixels in terms of the ratio of the actual dot radius to the ideal dot radius. Thus, the gray level for each pixel is entirely determined by the bits in a 3×3 window. They used the circular dot-overlap model in their modified error diffusion algorithm to obtain high quality reproductions [1] and for least-squares model-based halftoning, which makes use of a model for visual perception [2]. Pappas *et al*. proposed a printer model obtained from reflectance measurements of the gray level of various printed dot patterns [3]. Baqai and Alleback used a similar measurement-based printer model based on data collected from a high resolution scanner in their direct binary search algorithm [4]. In [2] and [4], an error between a perceived gray-scale image and the perceived printed image from a halftoned binary image is minimized. In all these methods, the accuracy and efficiency of the halftoning algorithm relies on the printer model's accuracy and performance.

The printer models discussed so far assume a constant gray level for a pixel. Although the eye responds only to the average gray level over the site, a measurable quantity such as reflectance must be examined in the continuous spatial domain in order to account for the complex interactions among dots. One such physical model is presented in [5]. This model can be extended to predict other development-related quantities such as gray value and Developed (toner) Mass/Area (DMA). A physical printer model suffers from one major disadvantage: It is computationally expensive since the physical equations, first of all, are fairly complex, and obtaining a reasonable average gray level for a pixel requires numerous calculation points per pixel; thus, it is not efficient to use such a physical model directly in digital halftoning algorithms.

Our approach is to use the physical model of [5] to train an adaptive signal processing model (SPM) offline. Once trained, the SPM can then be used in algorithms such as [1]-[4]. The SPM proposed in this paper is suitable for use with resolution doubling techniques [9], multi-level halftoning techniques, and traditional binary halftoning techniques.

A review of the physical model is presented in Section II. The SPM is described in Section III. Section IV presents our simulation results. The conclusions are summarized in Section V.

II. PHYSICAL MODEL

The physics of electrophotography has been presented in a number of publications, e.g., [6]-[7]. Given the latent image exposure, other physical quantities such as photoconductor voltage or developed toner mass per unit area (DMA) can be calculated [5]. Exposure seen at point (x, y) as a function of time t from the moment the laser turns on is given by

$$E(x,y,t) \equiv E_{on}(x,y,t_{on}) + E_{off}(x,y,t), \qquad (1)$$

where

This work was supported by Hewlett Packard Co., Contract No. KKK658.

$$E_{on}(x,y,t_{on}) \equiv \frac{P_t}{2\pi\alpha\beta} e^{-\frac{1}{2}(y/\beta)^2} * \int_0^{t_{on}} e^{-\frac{1}{2}((x-v\tau)/\alpha)^2} (1-e^{-\tau/t_r})\, d\tau \quad (2)$$

$$E_{off}(x,y,t) \equiv \frac{P_t}{2\pi\alpha\beta}(1-e^{-t_{on}/t_r})\, e^{-\frac{1}{2}(y/\beta)^2} * \int_{t_{on}}^{t} e^{-\frac{1}{2}(x-v\tau/\alpha)^2-(\tau-t_{on})/t_f}\, d\tau \quad (3).$$

P_t is the beam power at the PC surface, v is the laser scan velocity across the PC, α is the horizontal spot size parameter, β is the vertical spot size parameter, t_r is the rise time, t_f is the fall time, and t_{on} is the actual "on" time of the beam. Equations (1)-(3) describe a linear and shift-invariant system. Consequently, we may calculate the exposure for individual spots and superimpose these results to obtain arbitrary latent images. As this operation is quite straightforward, the SPM presented here deals only with single-spot exposure calculation. The exposure for a four-point font "w" character calculated using the exposure equations (1)-(3) is compared with the measured reflection density in Fig. 1.

In this paper, the SPM is trained offline, using the physical model, to approximate single-spot exposure. Any of a number of post-processing methods can then be used to transform the exposure to other development-related quantities. A good treatment of solid area development, which requires knowledge of the PC surface potential, can be found in [7]. The relationship between the PC surface potential and exposure is non-linear and very difficult to model analytically. Williams used the arctangent function to approximate the voltage [8]. Yi proposed a more empirical approach, where the exposure calculation and experimental data from an electrostatic voltmeter and a laser power modulator are utilized to predict the PC surface potential [5]. Similarly, a simple characteristic curve can be obtained using experimental data to convert exposure into its corresponding gray value or into its DMA. As an example, such an empirical relationship between exposure and gray value, using incremental gray scale images and the average exposure values from the physical model, is shown in Fig. 2. Finally, one can use the calculated electric field between the PC and the developer, based on the PC surface voltage, to estimate DMA. As an example, a comparison of measured DMA with the theoretical DMA of a 40 pixel × 40 pixel square, obtained using the field in the toner layer, is shown in Figs. 3.

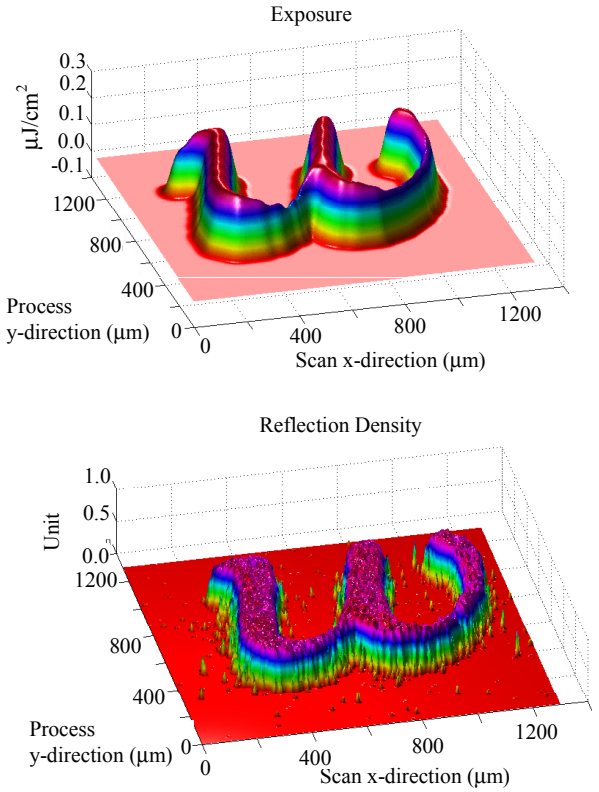

Figs. 1. Theoretical Exposure (top) and Measured Reflectance Density (bottom) for a 4-point "*w*" Character

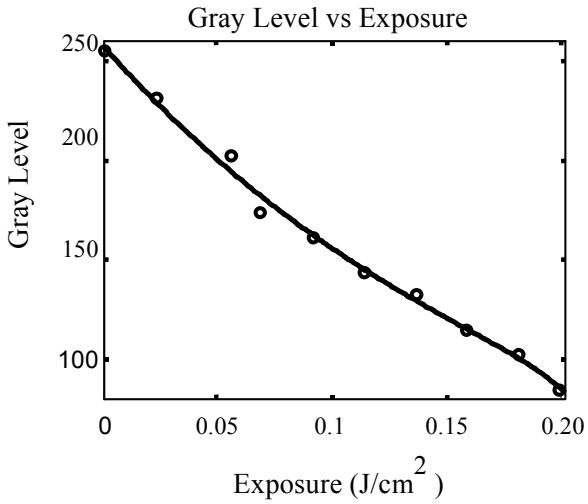

Fig. 2. Empirical relationship between exposure and gray level

III. SIGNAL PROCESSING MODEL

In most laser printers today, the laser pulse width within a pixel's boundary can be modulated to produce a smaller dot in the laser scan direction. For example, if a pixel is divided into 8 vertical sub-pulses (8-bit modulation), there are $2^8 = 256$ possible pulse time modulation (PTM) patterns. In practice, most print engines are constrained to generate a continuous pulse within a pixel's length. This reduces the number of possible exposure profiles to 36 plus a "zero -- modulation" case. After calculation, the profiles can be tabulated and looked up when a particular profile is needed [9].

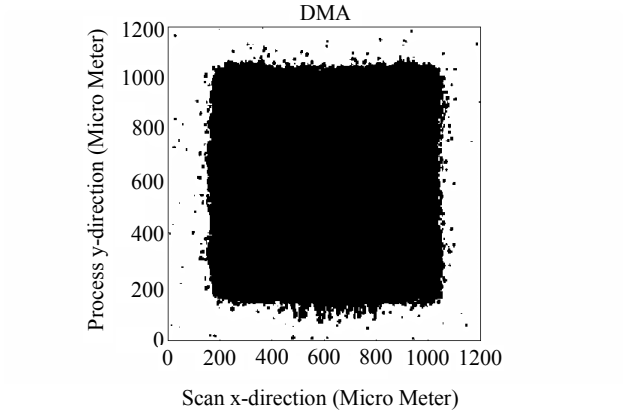

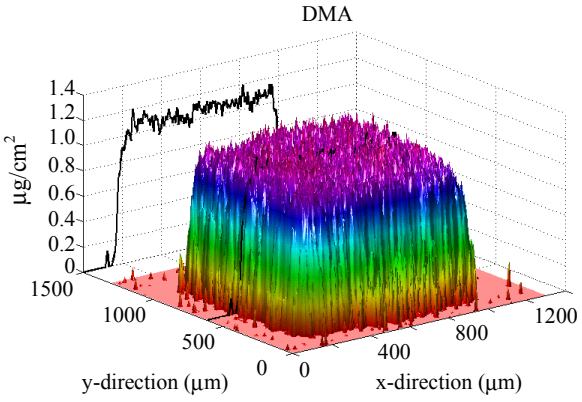

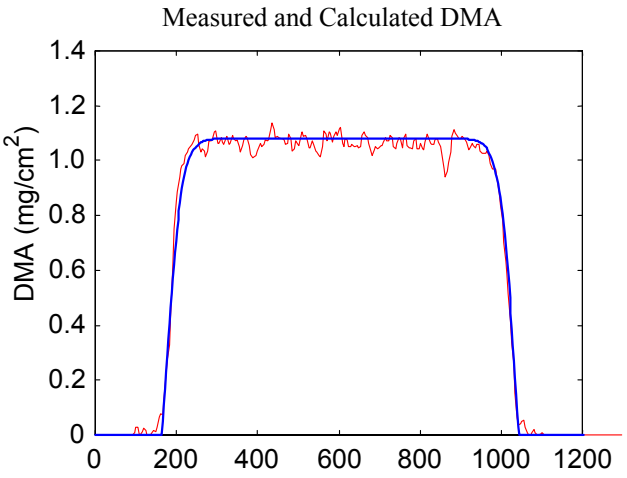

Figs. 3. Measured DMA for a 40×40 square (top), measured DMA with a cross section in x direction (middle), and the average of 5 measured DMA cross sections compared with calculated DMA (bottom)

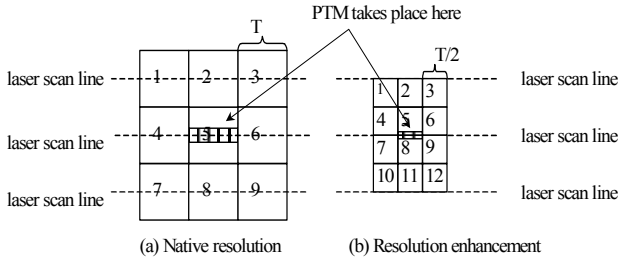

Fig. 4. Two Windows

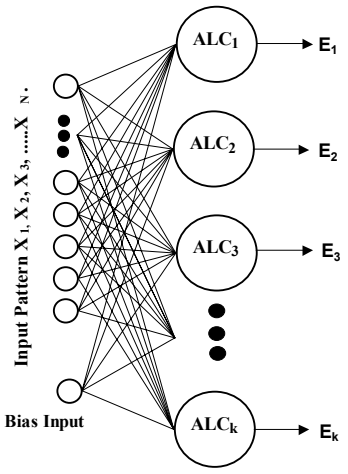

(a) One layer of ALCs

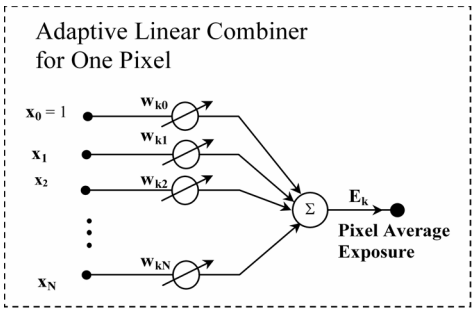

(b) A single adaptive linear combiner ALC_k

Fig. 5. The signal processing model SPM

Two windows are shown in Fig. 4. In Fig. 4(a), the scanning position of laser beam is at the center of the pixel. In this case, the size of one pixel represents the printer resolution (about 42 μm for a 600 dpi printer). To increase this optical resolution by a factor of two, one must be able to place two pixels between two scan lines where the PTM takes place, as illustrated in Fig. 4(b). The pixels between the scan lines are created by appropriately interleaving isolated exposure profiles [9]-[11].

For the experiments reported in this paper, the 4×3 window in Fig. 4(b) and 8-bit subpixel modulation were used. The window is divided into 12 square pixels and the system is trained with the average exposure value of each desired subpixel calculated by the physical model. The resulting isolated exposure profile consists of a modulation pattern and the average exposure value for each subpixel in the window.

The SPM is shown in Fig. 5. It consists of a layer of Adaptive Linear Combiners (ALCs) used to calculate average exposure in the pixel. There can be a significant variation in exposure at the subpixel-by-subpixel level depending on the PTM pattern. This variation can be characterized using the peak exposure to average exposure ratio (PAR).

Each ALC, shown in Fig. 5(b), produces an exposure output as

$$E_k = \sum_{n=0}^{N} x_n w_{k,n} \equiv \mathbf{X}^T \mathbf{W}_k \,, \qquad (4)$$

where E_k is the exposure output of ALC_k, $w_{k,n}$ is the nth weight of ALC_k, $x_n \in \{-1, +1\}$ for each timeslot in the pixel, $\mathbf{X} = [1\ X_1\ \cdots\ X_N]^T$, and $\mathbf{W}_k = [w_{k,0}\ w_{k,1}\ \cdots\ w_{k,N}]^T$. By convention, $x_0 = +1$ is a bias input bit. Each ALC is trained with the well-known μ-Least Mean Squared (μ-LMS) algorithm

$$\mathbf{W}_k^{(t+1)} = \mathbf{W}_k^{(t)} + 2\mu\left(E_k^{(t)} - d_k^{(t)}\right)\mathbf{X}^{(t)}, \qquad (5)$$

where t is the iteration index, $d_k^{(t)}$ is the average exposure of the kth pixel (corresponding to ALC_k) from the physical model using the input $\mathbf{X}^{(t)} = [1\ X_1^{(t)}\ \cdots\ X_N^{(t)}]^T$, $\mathbf{W}_k^{(t)} = [w_{k,0}^{(t)}\ w_{k,1}^{(t)}\ \cdots\ w_{k,N}^{(t)}]^T$ is the weight vector for ALC_k, and μ is the adaptation constant [12]. The number of inputs for each ALC is equal to the number of modulation pattern bits plus one bias input bit. One ALC per pixel is required.

In applying the SPM after completion of offline training, we calculate exposure for each given spot, superimpose the exposure results, and map the exposure to the desired quantity, e.g., reflectance, DMA, etc. This process can be illustrated as follows.

Table 1 shows 4 examples of isolated exposure profiles. The pixel number in Table 1 corresponds to the pixel's position in Fig. 4(b). The modulation pattern encodes the 8-bit PTM applied to the center of the window, as shown in Fig. 4(b). A pixel's length is divided into 8 sub-pulses in the scan direction. The laser beam is on when the bit is "1"and it is off when the bit is "0". Each pattern has a unique set of average exposure values.

Fig. 6 shows an example of the total average exposure values that are the result of linear superposition of the isolated exposure profiles in Table 1 using the window in Fig. 4(b). Hexadecimal patterns, 80 and C0, are placed on the upper scan line, and patterns, 03 and FF, are placed on the lower scan line. Compared to the isolated exposure in Table 1, the total exposure in the pixels between two scan lines are significantly greater due to the dot-overlap.

The total exposure value in each pixel is critical to whether or not toner development takes place in a pixel. There is a critical point in the development process at which toner development starts to take place. This development threshold for the printer to be modeled can be determined experimentally. Visible development for a test print engine in our laboratory begins to take place when the exposure reaches about 0.01 μJ/cm^2. Thus, model error of a few percent in a pixel where the exposure is far below the threshold can be ignored for all practical purposes. Similarly, at exposures well above threshold, model error is again negligible due to saturation effects in toner development. Typically, tolerances for various printer parameters such as laser power and spot parameters range 5-10 percent. Based on these considerations, we will consider a model standard error of 5 percent to be tolerable for the SPM.

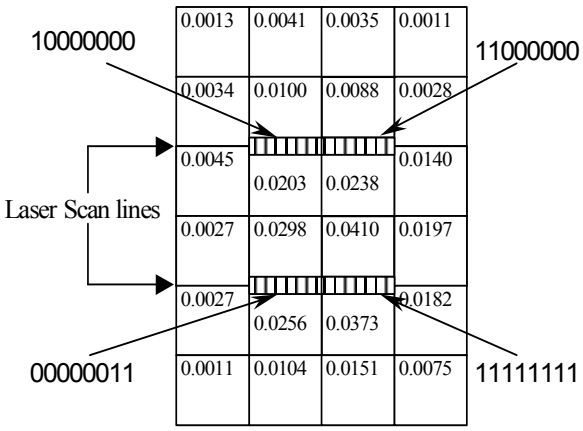

Fig. 6. Total Average Exposure Value

Table 1. Examples of Isolated Exposure Profiles

Modulation Pattern		10000000	11000000	00000011	1111111
Hex No.		80	C0	03	FF
Average Exposure Value of Pixel (μ Joules/cm^2)	Pixel No. 1	0.0013	0.0026	0.0011	0.0073
	2	0.0015	0.0030	0.0030	0.0124
	3	0.0005	0.0011	0.0026	0.0075
	4	0.0034	0.0064	0.0027	0.0182
	5	0.0036	0.0075	0.0074	0.0308
	6	0.0013	0.0028	0.0065	0.0185
	7	0.0034	0.0064	0.0027	0.0182
	8	0.0036	0.0075	0.0074	0.0308
	9	0.0013	0.0028	0.0065	0.0185
	10	0.0014	0.0026	0.0011	0.0074
	11	0.0016	0.0031	0.0030	0.0125
	12	0.0006	0.0012	0.0026	0.0075

IV. RESULTS

The training and test results shown in Table 2 consists of five major rows: Experiment, PAR, Training Data, Test Data, and All Data. The first major row (Experiment) describes each experiment, including the number of training patterns and test patterns. The second major row is the Peak to Average Ratio (PAR). PAR is the maximum exposure value in a subpixel divided by the average exposure value of the subpixel as calculated from the physical model. PAR indicates how much the exposure deviates within a pixel. PAR = 1.0 means that the average exposure is representative of the exposure throughout the region. On the other hand, if PAR is much greater than 1.0, the average value is significantly different from the maximum exposure elsewhere within the region. The third major row shows the average percent error and its standard deviation using the training patterns with respect to the exposures calculated using the physical model. The fourth row gives the error statistics for the test patterns (patterns that are not used in training). The fifth row shows the error statistics taken over all 255 possible patterns. Three experiments are conducted using 256 (E1), 37 (E2), and 16 (E3) training patterns, which corresponds to 0, 219, and 240 test patterns, respectively. These results illustrate the effect of the number of training patterns on the accuracy of the SPM. The key points here are accuracy, the efficiency of training the SPM, and calculation performance. The average percent errors for these experiments are negligibly small (their magnitude is less than 0.01 %) and so the aforementioned accuracy criteria is met.

Table 2. ALC training results

Experiment	Experiment No.	E1	E2	E3
	Number of Training Patterns	256	37	16
	Number of Test Patterns	0	219	240
PAR	Avg PAR	1.8306	1.8306	1.8306
	Std Dev (PAR)	0.3873	0.3873	0.3873
Training Data	Avg % Error	6.695E-08	-1.25E-06	-7.68E-07
	Std Dev (% Error)	3.453E-06	4.95E-06	5.18E-06
Test Data	Avg % Error	NA	-5.12E-07	-3.04E-07
	Std Dev (% Error)	NA	2.35E-06	1.91E-06
All Data	Avg % Error	6.695E-08	-6.16E-07	-3.32E-07
	Std Dev (% Error)	3.453E-06	2.87E-06	2.24E-06

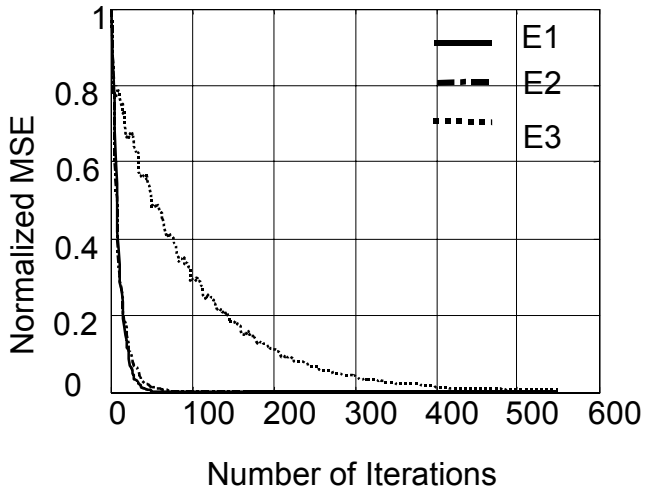

Fig. 7. Learning Curves of E1, E2 and E3. The vertical axis is the Nomalized MSE and the horizontal axis is the number of training cycle iterations.

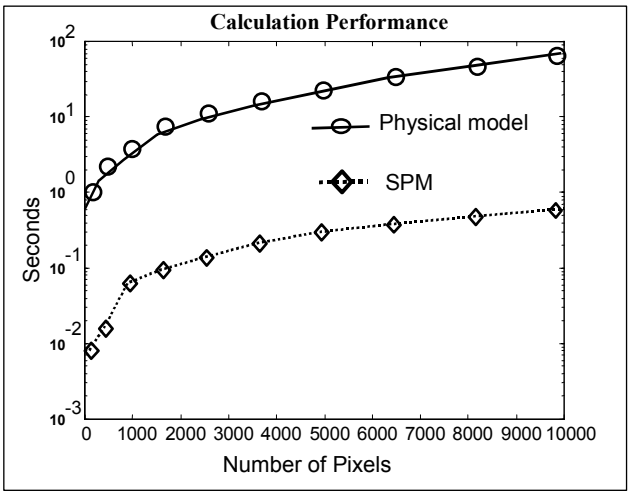

Fig. 8. Calculation Performance of SPM and Physical Models

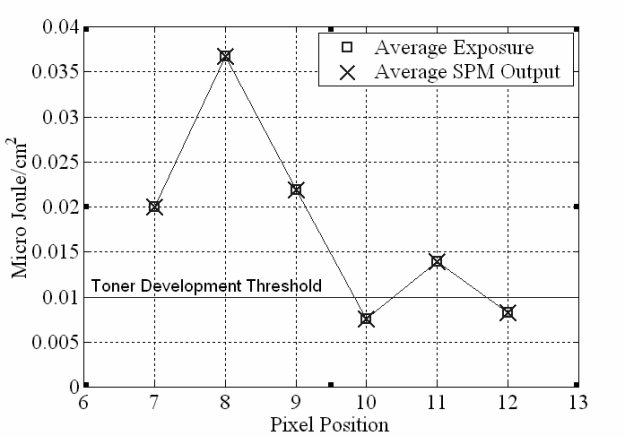

Fig. 9. The average exposure from the physical model, and average exposure from the SPM for E3. The pixel position corresponds to the pixel number in Fig. 4(b). Pixels 1 through 6 are not shown because these curves are symmetric about the scan line in the window.

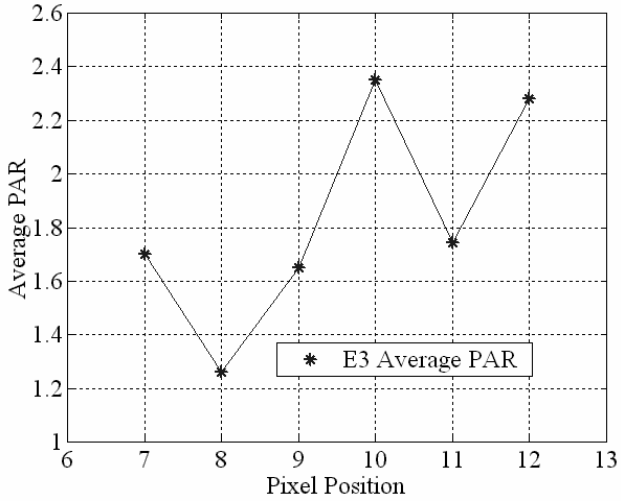

Fig.10. Average PAR for E3

Since using more training patterns requires more physical model calculations and does not affect the results, we recommend using the minimum number of training patterns (case E3). The mean-squared error (MSE) learning curves for E1, E2 and E3 are shown in Fig. 7. The curves are normalized to an initial MSE of one. The learning curve for E3 converges more gradually than the MSE of E1 and E2 due to the small number (16) of training patterns. Once trained, the SPM's performance is two orders of magnitude better than the physical model, as shown in Fig. 8 where the performance (calculation time in seconds) of the two models are compared against varying numbers of processed pixels. The average exposure for each pixel in E3 is shown in Fig. 9. These results are obtained from all 255 possible modulation patterns. The exposure at the scan line (Pixel 8 in Fig. 9) in the middle of the window, where the PTM takes place, reaches its maximum and exceeds the development threshold. The exposure in the corner pixels (Pixels 10 and 12) is the smallest in the window.

Of interest here is the Peak to Average Ratio (PAR) characteristics of the model. All else being equal, smaller PAR values are preferable to larger ones. The average PAR of each pixel in E3 is shown in Fig. 10. The PAR ranges from 1.2 to 2.4 in the window. The smallest PAR (1.2) is observed when the average exposure is largest in the window, whereas the PAR reaches its maximum (2.4) in the corner pixels. This indicates that, using one ALC/pixel, the SPM can accurately predict the average exposure of the pixels whose average exposure exceeds the development threshold, while its outputs for the corner pixels will not be as representative of those pixels.

V. SUMMARY AND CONCLUSIONS

We demonstrated that an accurate printer model that is efficient enough to be used in halftoning can be obtained by training the SPM from a physical printer model using the μ-LMS algorithm. The SPM is trained once offline, after which the average exposure of each subpixel for any input pattern can be calculated in real time. Experimental results reported in this paper verified that the exposure obtained from using the SPM and the average exposure from the physical model are in good agreement.

VI. REFERENCES

[1] T. N. Pappas and D. L. Neuhoff, "Printer models and error diffusion," *IEEE Trans. Image Processing*, vol. 4, pp. 66-80, Jan. 1995.

[2] T. N. Pappas and D. L. Neuhoff, "Least-squares model-based halftoning," *IEEE Trans. Image Processing*, vol. 8, pp. 1102-1116, Aug. 1999

[3] T. N. Pappas, C. Dong, and D. L. Neuhoff, "Measurement of printer parameters for model-based halftoning," *J. Electron. Imaging*, vol. 2, no. 3, pp. 193-204, Jul. 1993.

[4] F. A. Baqai and J. P. Alleback, "Printer models and the direct binary search algorithm," *Proc. 1998 IE International Conference on Acoustics, Speech, and Signal Processing*, vol. 5, 1998.

[5] J. Yi, "A xerographic simulation model," M.S. thesis, University if Idaho, Moscow ID, May 1999.

[6] E. M. Williams, *The physics and technology of xerographic processes*. Malaba, Florida: Krieger Publishing Company, 1993

[7] L. B. Schein, *Electrophotography and development physics*. Morgan Hill, California: Laplacian Press, 1992

[8] E. M. Williams, "Electrostatic field of arctangent voltage transitions in elctrophographic images," *Photographic Science and Engineering*, vol. 26, no. 2, pp. 88-91, March/April. 1982.

[9] DP-Tek, Inc., Resolution transforming raster-based image system, United States Patent # 5,134,495, Jul. 28,1992.

[10] DP-Tek, Inc., Interleaving vertical pixels in raster-based laser printers, United States Patent # 5,193,008, Mar. 9,1993.

[11] DP-Tek, Inc., System and method for enhancing graphic features produced by making engines, United States Patent # 5,515,480, May. 7,1996.

[12] B. Widrow and M. A. Lehr, "30 years of adaptive neural networks: perceptron, madaline, and backpropagation," *Proc. IEEE*, vol. 78, no. 9, pp. 1415-1442, Sept. 1990